SUPPORTING INFORMATION

The role of Eudragit® as a component of hydrogel formulations for medical devices

David Esporrín-Ubieto[1], Ana Sofía Sonzogni[2], Mercedes Fernández[3], Arantxa Acera[4,8], Eider Matxinandiarena[5], Juan F. Cadavid-Vargas[6], Itxaso Calafel[3], Ruth N. Schmarsow[7], Alejandro J. Müller[5,8], Aitor Larrañaga[9], Marcelo Calderón[1,8, *]

[1]POLYMAT, Applied Chemistry Department, Faculty of Chemistry, University of the Basque Country UPV/EHU, Paseo Manuel de Lardizabal 3, 20018 Donostia-San Sebastián, Spain.

[2]Group of Polymers and Polymerization Reactors, INTEC (Universidad Nacional del Litoral-CONICET), Güemes 3450, 3000 Santa Fe, Argentina.

[3]POLYMAT Institute for Polymer Materials, University of the Basque Country UPV/EHU, San Sebastián, 20018, Spain.

[4]Department of Cell Biology and Histology, Experimental Ophthalmo - Biology Group (GOBE, www.ehu.eus/gobe), University of the Basque Country UPV/EHU. Bº Sarriena, sn, 48940 Leioa, Bizkaia, Spain.

[5]POLYMAT, Department of Polymers and Advanced Materials: Physics, Chemistry and Technology, University of the Basque Country UPV/EHU, Paseo Manuel de Lardizábal 3, 20018 Donostia-San Sebastián, Spain.

[6]INIFTA-CONICET-UNLP, Instituto de Investigaciones Fisicoquímicas Teóricas y Aplicadas, Diagonal 113 y 64, 1900 La Plata, Argentina.

[7]Institute of Materials Science and Technology (INTEMA), University of Mar del Plata and National Research Council (CONICET), Av. Cristóbal Colón 10850, 7600 Mar del Plata, Argentina.

[8]IKERBASQUE, Basque Foundation for Science, Plaza Euskadi 5, 48009 Bilbao, Spain.

[9]Department of Mining, Metallurgy Engineering and Materials Science, POLYMAT, Faculty of Engineering in Bilbao, University of the Basque Country (UPV/EHU), Plaza Torres Quevedo 1, 48013 Bilbao, Spain.

*Author for correspondence: marcelo.calderon@polymat.eu

INDEX

S1. Dynamic oscillatory viscoelastic analysis

We conducted dynamic oscillatory rheological analysis on unhydrated hydrogels A – E, enabling the elucidation of the temperature's impact on their structures at the dynamic molecular level. Employing this experimental approach, we subjected the materials to compression deformation using a dynamic oscillatory mode, maintaining a constant frequency of 1 Hz while sweeping through various temperatures. Through this comprehensive assay, we were able to dissect thermal transitions and differentiate the elastic behaviour intrinsic to the hydrogel structure from the deformation arising over time due to viscous dissipation. The outcomes of this investigation are visualized in **Figure S1**, where the results for the storage modulus G' (**Figure S1A**), loss modulus G'' (**Figure S1B**), and the Tan δ loss tangent (**Figure S1C**) are presented.
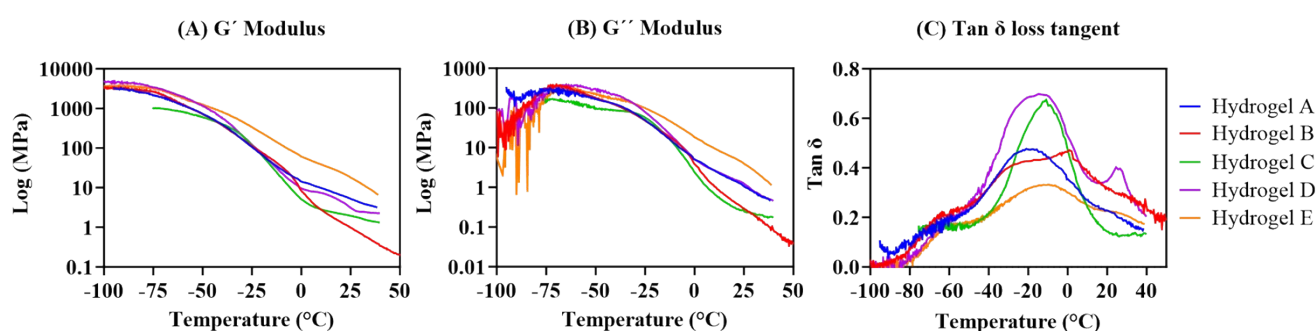

Figure S1. Dynamic viscoelasticity analysis depicting the evolution of (A) storage modulus G', (B) loss modulus G'', and (C) tan δ loss tangent at various temperatures and a consistent 1 Hz oscillation frequency during compression.

Our observations from **Figure S1A** and **B** underscore that the storage modulus (G') and loss modulus (G'') manifest solely at temperatures below 0 °C, reaching their peak magnitudes within the range of -50 to -70 °C. Notably, at these ultra-low temperatures, the storage modulus (G') exhibits substantial values, spanning the order of megapascals (MPa). As temperature increases, this modulus experiences a gradual decline due to heightened molecular mobility resulting from increased thermal energy. These behaviour strongly aligned with a gelled system characterized by rigid structures. The diminishing trend in both moduli signifies a softening of the hydrogels at elevated temperatures. It is noteworthy that among the five hydrogels, hydrogel C (distinguished by green lines) demonstrates notably lower values for both G' and G''. This observation designates hydrogel C as the most pliant among the group.

Figure S1C illustrates the presentation of the tan δ loss tangent, a parameter instrumental in establishing the glass transition temperature (Tg) for each hydrogel. The Tg is identified as the peak value of the tan δ curve. This pivotal temperature signifies the point at which the amorphous polymer structure transitions from a "hard glassy" state to a aoft/rubbery state, reflecting a significant change in material properties. Summarizing the Tg values for hydrogels A – E, **Table S1** consolidates this crucial data, offering a comprehensive overview of the temperature regimes at which these transitions occur. This analysis not only deepens our understanding of the hydrogels' dynamic behaviour but also sheds light on their fundamental material transformations.

Table S1. Tg values for hydrogel A – E obtained from Figure S1C after compression dynamic oscillatory rheology analysis.

Hydrogel	Tg (°C)
A	-19
B	1
C	-11
D	-15
E	-10

As evident from the data presented in **Table S1**, it becomes apparent that altering the Eudragit type directly influences the Tg value. Remarkably, however, all these values consistently fall below 37 °C, the standard body temperature. Consequently, regardless of the Eudragit variant utilized, it is evident that all these materials are characterized by a viscous structural state when employed for biomedical applications. This consistent behaviour further reinforces their suitability for various medical contexts.

In the context of this study, the polymers under examination—namely, PVA, PVP, PEG, and Eudragit—exhibit a pivotal interconnection through hydrogel bonds. These bonds, stemming from the abundance of oxygen and hydrogen atoms, serve as the most significant junctures for cross-linking. Taking PVA as a prime example, its hydroxy group within its molecular structure facilitates self-interaction, enabling the formulation of hydrogels exclusively grounded in PVA. This pioneering feature was initially documented by Peppas in 1975.[1] More

contemporarily, a synergistic approach melds PVA with PVP, fostering the stability of the hydrogel through the establishment of interchain hydrogen bonding, as elucidated by Palmese et al.[2] Furthermore, certain publications have underscored that during the process of gel formation, cross-linking points arise between the hydroxy groups of the PVA and the carboxyl groups of the PVP.[3] Notably, the combination of PVA and PEG also stands out, yielding physically cross-linked hydrogels that achieve a notable interaction yield of approximately 60%.[4] This achievement is credited to the hydrogen bonds that materialize between the distinct polymeric chains. Ultimately, analogous hydrogen bonds can also be established with the oxygen groups inherent in the chemical structure of Eudragit polymers.

S2. NMR spectra of the polymers that composed the five different hydrogels dissolved in BSS solution.
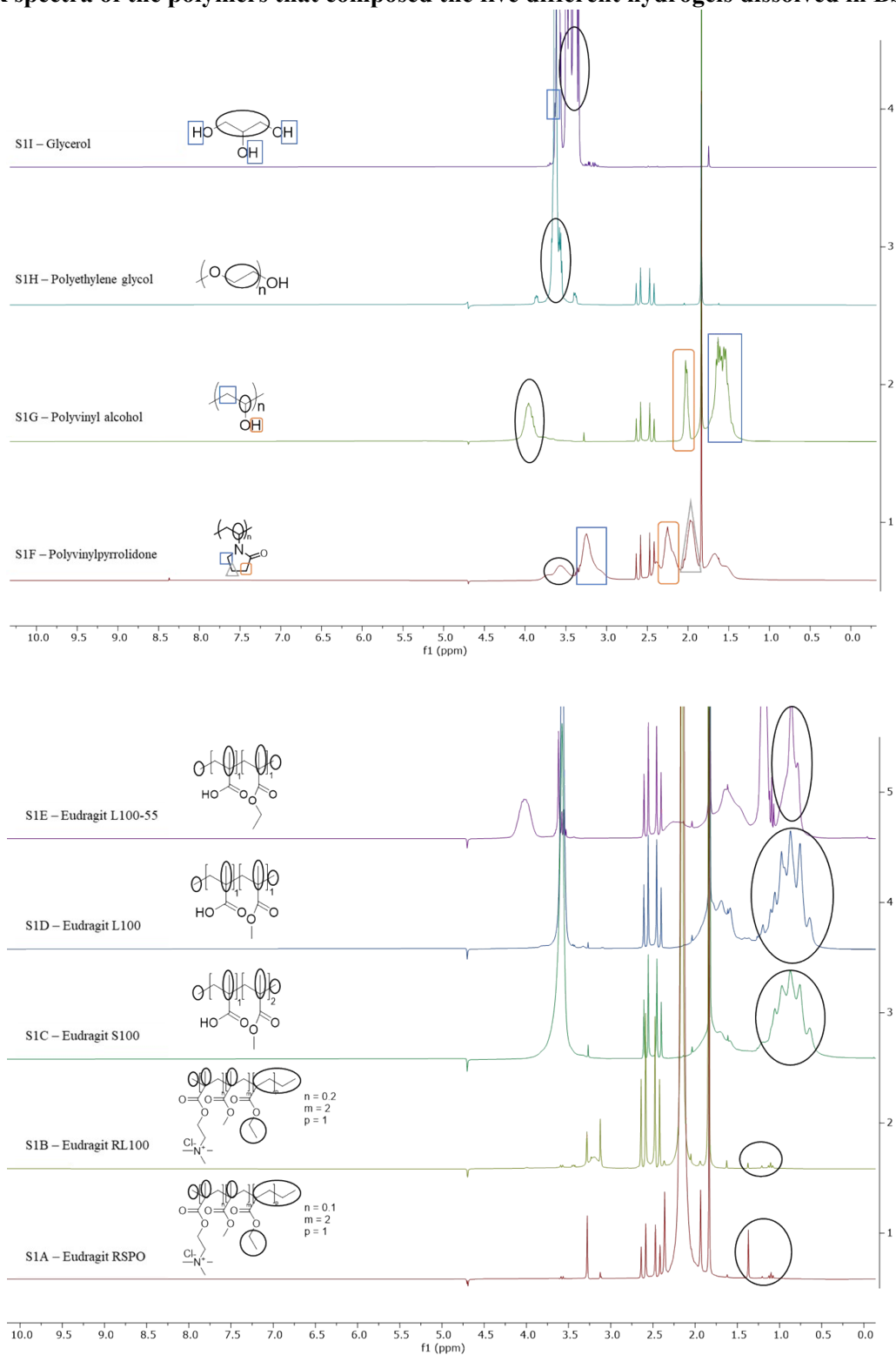

Figure S2. ^{1}H-NMR (300 MHz, BSS/D$_2$O 90/10) spectra of all the polymers involved in the different hydrogels. S1A Eudragit RSPO, S1B Eudragit RL100, S1C Eudragit S100, S1D Eudragit L100, S1E Eudragit L100-55, S1F Polyvinylpyrrolidone, S1G Polyvinyl alcohol, S1H Polyethylene glycol, S1I Glycerol.

S3. Moisture content and moisture uptake studies

Hydrogels are known for their remarkable ability to retain water within their matrices. However, as the materials studied in this research are physically cross-linked, they have a maximum water retention capacity beyond which they lose their structural integrity. At this point, the polymers that form the hydrogel start dissolving into the absorbed water. To gain insight into the stability of the matrix under humid conditions, moisture uptake (MU) and moisture content (MC) were analysed using a previously reported protocol with minor modifications.[5] The hydrogels samples were placed inside a desiccator (as shown in **Figure S3**) and subjected to either a saturated solution of potassium sulphate, K_2SO_4 (MU), which provides an ambient humidity of 97%, or silica gel (MC).
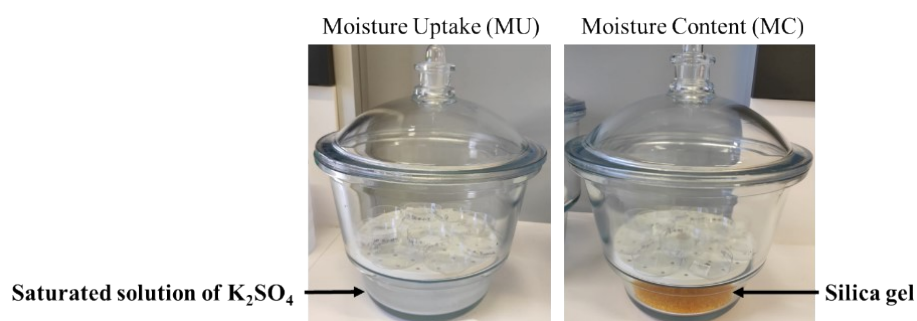

Moisture Uptake (MU)   Moisture Content (MC)

Saturated solution of K_2SO_4 →   ← **Silica gel**

Figure S3. Samples of 1 x 1 cm from hydrogels A-E inside of a desiccator. Moisture uptake assay (with a saturated solution of K_2SO_4, 95% relative humidity) and moisture content (with silica gel).

The K_2SO_4 solution used in the MU study generates an atmosphere with a relative humidity of 97%, which causes the hydrogel matrices to absorb water from the environment. Consequently, the weight of the hydrogels will increase until they reach their maximum water retention capacity. Beyond this point, the hydrogels will dissolve, reducing their stability. In contrast, in the MC study, silica gel absorbs water from the environment, causing the water retained inside the matrices to be removed. This results in a decrease in the weight of the hydrogel due to the loss of water. **Figures S4A** and **S4B** depict the results obtained from the MC and MU analyses.
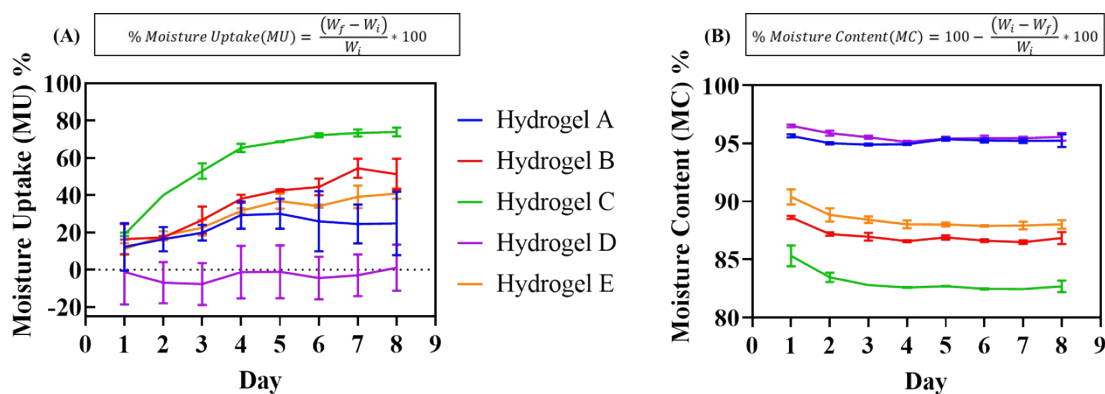
Figure S4. (A) Percentage of moisture uptake for all hydrogels vs. time. (B) Percentage of moisture content for all hydrogels vs. time. W_i represents the initial weight; W_f is referred to the final weight. (N = 3)

Figure S4A presents the results of the MU analysis, which revealed three distinct types of behavior among the hydrogels studied. The first type involves a hydrogel that is already fully swollen and cannot absorb any more water. Consequently, it starts dissolving in the humidity in the environment, causing the hydrogel to lose weight (hydrogel D). Conversely, the second type is characterized by a hydrogel that continues to absorb water for more than a week, resulting in a steady increase in weight (hydrogel C). The remaining hydrogels (A, B, and E) displayed intermediate behaviours. These materials could absorb water for a few days but eventually lose weight due to the dissolution of polymeric chains in the environmental humidity.

As previously described, hydrogel D has already reached its maximum water retention capacity and cannot absorb more water. As shown in plot **S4A**, the MU for hydrogel D is negative, indicating that the hydrogel loses weight throughout the entire experiment. Since the hydrogel cannot absorb any more water, the humidity present in the K_2SO_4 solution is instead being used to dissolve the hydrogel, thereby compromising the matrix's stability in humidity.

In the second scenario, hydrogel C exhibits the greatest swelling capacity without compromising the matrix stability. Material C can continue to absorb water for up to 7 - 8 days, gradually increasing its MU. Therefore, hydrogel C is the only one among the five materials studied that can retain a greater amount of water while maintaining its integrity in the presence of a relative humidity of 97% for a longer duration.

The third scenario represents an intermediate situation between the two previously described ones. In this case, hydrogels A, B, and E can absorb water from the environment and maintain their matrix stability for a few days.

However, the materials lose weight after this initial period, and the matrix stability is subsequently compromised. For instance, hydrogels A and E can absorb water for 4 - 5 days before their MU decreases, reducing the material's stability. On the other hand, hydrogel B can retain water and preserve the matrix stability for up to 7 days before the MU begins to decrease.

The experiment suggests that the water retention capacity of hydrogels A – E is influenced by the type of Eudragit used. Hydrogel C, which is based on Eudragit S100, can retain the highest amount of water. This particular Eudragit is soluble in water at physiological pH, but the acidic pH of the humidity created by K_2SO_4 may prevent its solubility, which could explain why it retains more water than the other hydrogels while remaining stable. The other hydrogels exhibited different swelling and dissolution behaviours that require further investigation. Nevertheless, the varying properties of the Eudragits® have significantly impacted the overall swelling capacity of the hydrogel matrix. A more advanced NMR-based swelling study has been performed to understand better these differences, detailed in section **3.3** of the main text.

Figure S4B summarizes the MC of materials A – E. The plot shows that all materials experienced a consistent water loss from their internal matrices over 3 – 4 days. The MC decay slope for hydrogels A – E was steeper during the first 4 days, indicating a significant water loss during this period. Analysing the difference between the initial and final water percentages for each material revealed differences between them. For instance, hydrogel A (based on Eudragit RSPO) and B (based on Eudragit RL100) decreased in MC of 0.625% and 2.44%, respectively. Considering the chemical structures of both Eudragits, it is noteworthy that while both are non-water soluble, RL100 is more polar than RSPO due to the greater number of repeating units in its quaternary amine group. This fact suggests that hydrogel B is expected to retain more water than hydrogel A, consistent with the MC results.

The remaining three materials, hydrogels C, D, and E, are made up of water-soluble polymers. The percentage of MC for each of these materials (initial minus final) is 3.2%, 1.8%, and 3.13%, respectively. Hydrogels C and E retain more water than hydrogels A and B, likely due to the presence of water-soluble polymers. Hydrogel D, on the other hand, only has a water retention of 1.8%, which is unexpected given the similar composition of hydrogels C and E. However, the lower MC value for hydrogel D is attributed to the material's stability and homogeneity. Based on Eudragit water-soluble at pH > 6, hydrogel D does not mix well with the other polymers

in the matrix, leading to phase separation during the drying process. This results in an inconsistent formulation and characterization of the material, making it difficult to reproduce reliably.

S4. Thermal and X-ray diffraction characterization for hydrogel's opacity comprehension
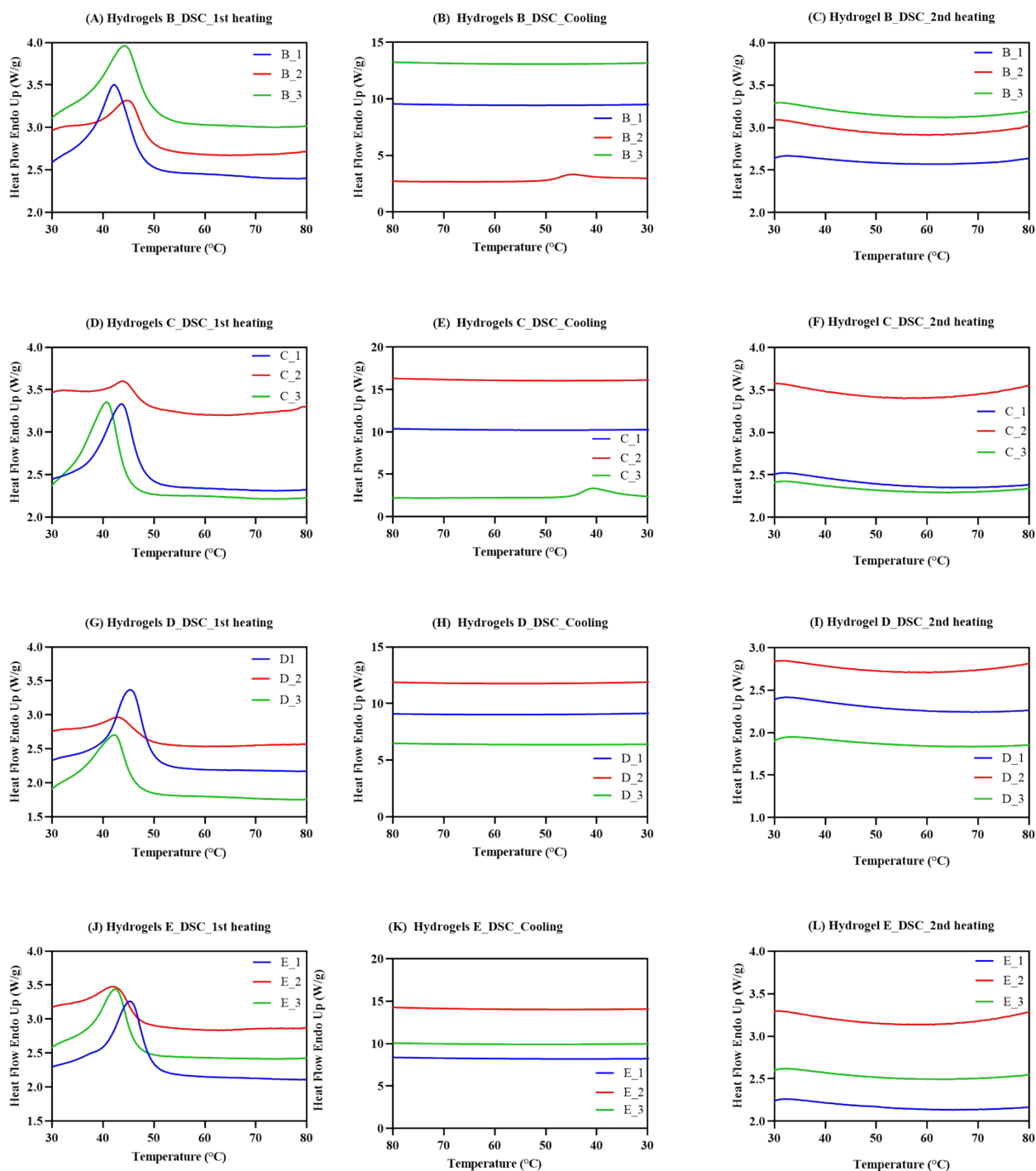## S4.1 Differential Scanning Calorimetry

Figure S5. X_1 empty hydrogel. X_2 hydrogel with BSA. X_3 hydrogel with BSA-FITC. (A, D, G, J) First heating DSC scans for hydrogels B, C, D, and E respectively. (B, E, H, K) DSC cooling scans for hydrogels B, C, D, and E, respectively. (C, F, I, L) Second heating DSC scans for hydrogels B, C, D, and E, respectively. Heating and cooling rate for all cases is 20 °C.

Table S2. Summary of the maximum temperatures of the endothermic peak (Tp) and the observed enthalpy of the endothermic transition (ΔHp) for hydrogels B – E. X_1 empty hydrogel. X_2 hydrogel with BSA. X_3 hydrogel with BSA-FITC. Data obtained from DSC analysis.

Sample Code	Tp, peak (°C) (1st heating)	ΔH$_p$ (J/g)
Hydrogel A_1	50.1	24.8
Hydrogel A_2	43.6	4.8
Hydrogel A_3	42	16.1
Hydrogel B_1	42.4	19.4
Hydrogel B_2	44.9	9.5
Hydrogel B_3	44.4	17.5
Hydrogel C_1	43.7	19.6
Hydrogel C_2	43.9	5.3
Hydrogel C_3	40.7	24.7
Hydrogel D_1	45.4	21.9
Hydrogel D_2	42.9	7.9
Hydrogel D_3	42.3	22.2
Hydrogel E_1	45.4	20.2
Hydrogel E_2	42.3	15.5
Hydrogel E_3	42.4	17.4

The second heating scan of the DSC analysis in **Figure S5 C**, **F**, **I**, **L** does not exhibit any peaks, which is consistent with hydrogel A's behaviour. Similar to the previous case, the hydrogels require more time to reform the matrix after the first heating scan. However, the first heating scan (**Figure S5 A**, **D**, **G**, **J**) displays peaks for both empty hydrogels B - E and those containing BSA and BSA-FTIC. Therefore, it can be confirmed that the primary transition observed in these samples under these conditions was related to the heat exchange during the crystal melting process and the gel-sol transitions. These crystals are believed to have emerged during the gelation process and likely contribute to the opacity seen in the hydrogels.

The results presented in **Table S2** demonstrate a similar trend in enthalpy values for hydrogels as observed for hydrogel A. Encapsulation of BSA inside the hydrogels leads to a significant reduction in the enthalpy of the endothermic transition compared to empty hydrogels (B - D samples). In hydrogel B, the enthalpy decreases

from 19.4 to 9.5 J/g. In hydrogel C, the enthalpy drops from 19.6 to 5.3 J/g. For hydrogel D, the enthalpy decreases from 21.9 to 7.9 J/g. However, hydrogel E only shows a slight decrease in enthalpy from 20.2 to 15.5 J/g. These results reaffirm that the enthalpy endotherms are also influenced by a combination of melting crystals and gel-sol transitions, as observed for hydrogel A.

However, we need to ensure that the measured enthalpies correspond to the melting of crystals or sol-gel transitions since crystals may also form during the gelation process, specifically composed of PVA and PEG. The literature reports that these polymers form crystals with melting endotherms of 138.60 J/g (PVA) and 173.21 J/g (PEG).[7,8] However, the low PVA and PEG fractions in the sample, compared with the large peaks in **Figures 9** and **S5**, indicate that the contribution of the sol-gel transition to the melting endotherms is much more significant than the contribution of the crystals. Hence, it is not possible to determine the crystal fractions from DSC data. Nevertheless, note that when adding BSA to the hydrogel, the enthalpy of melting endotherms is reduced from 24.8 to 4.8 J/g because BSA is highly hydrophilic (water solubility 40 g/L), increasing the solubility of the hydrogel and decreasing hydrophobic interactions. Conversely, when BSA is chemically combined with FITC, the hydrogel becomes less soluble, increasing the enthalpy of the endothermic transition to 16.1 J/g. These results indicate that the presence of hydrophobic molecules during gelation increases the endothermic transition's enthalpy.
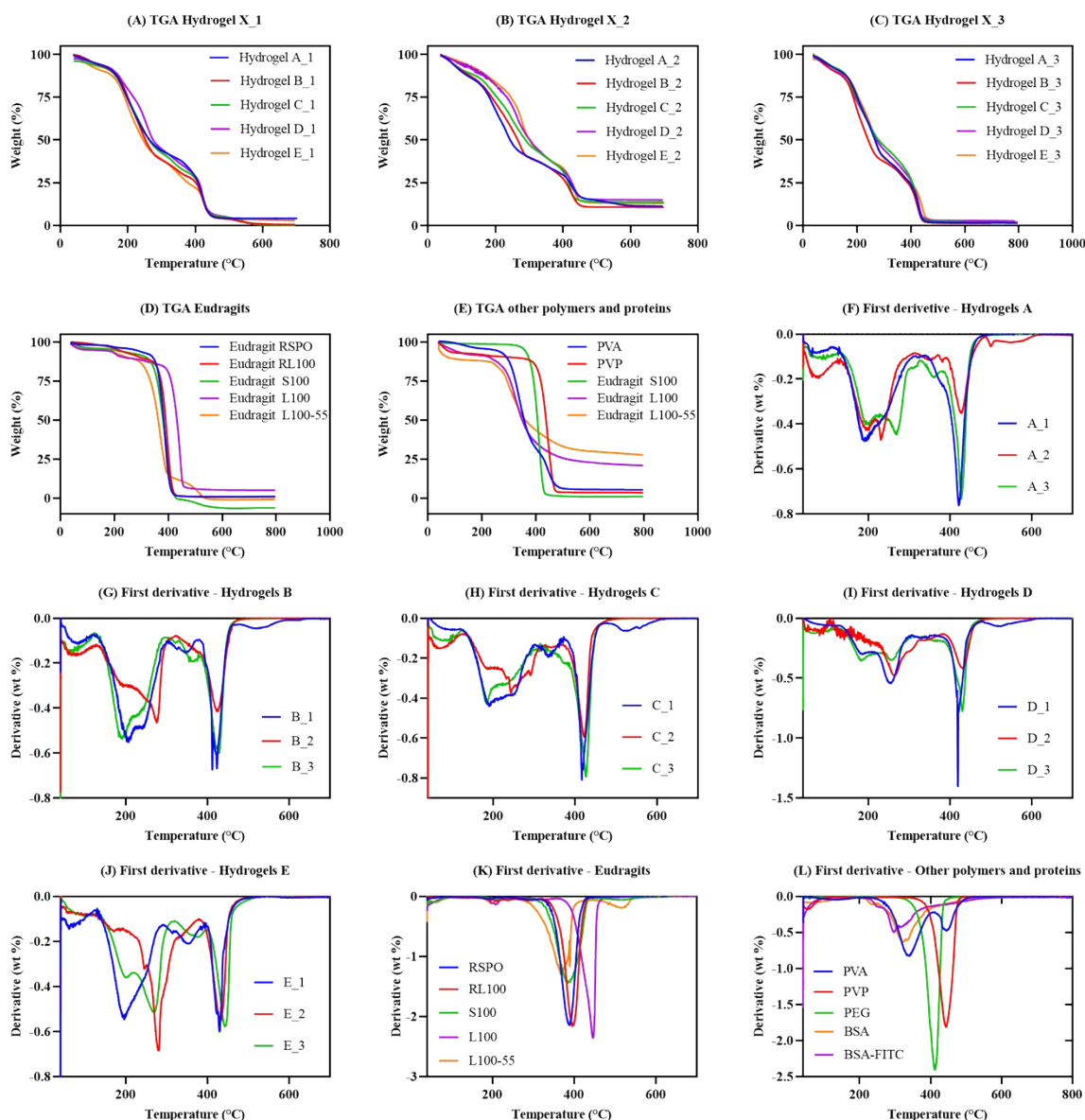
S4.2 Thermogravimetric analysis

Figure S6. (A – E) TGA plots for hydrogels A – E in three scenarios. (A) Empty hydrogels. (B) Hydrogels with BSA. (C) Hydrogels with BSA-FITC. (D) Eudragits as controls. (E) Rest of the polymers and proteins used for hydrogel preparation. (F – J) First derivative of the TGA curve for the hydrogels A -E. (X_1) Empty hydrogels. (X_2) Hydrogels with BSA. (X_3) Hydrogels with BSA-FITC. (K) First derivative of the TGA curve for Eudragits pure polymers. (L) First derivative of the TGA curve for the rest of the polymers and proteins used for hydrogel's preparation.

Table S3. Summary of the temperatures at which 5, 10, and 50% of the total weight has been lost. Data is shown for Hydrogels A – E in the three scenarios. (1) Empty hydrogels. (2) Hydrogels with BSA. (3) Hydrogels with

BSA-FITC. Besides, a summary of the temperatures from the maximum peak obtained from the first derivative of the TGA curve is also shown.

Sample Code	T (°C): Loss 5 % of Weight	T (°C): Loss 10 % of Weight	T (°C): Loss 50 % of Weight	First derivative – Max. Peak region 1 / T (°C)		First derivative – Max. Peak region 2 / T (°C)
Hydrogel A_1	111.6	156.2	264.7	190	-	420
Hydrogel A_2	71.2	99.5	243.8	198	231	426
Hydrogel A_3	85.4	138.9	267.2	195	266	427
Hydrogel B_1	100	154.1	252.5	205	-	423
Hydrogel B_2	71.5	104.3	266.3	275	-	422
Hydrogel B_3	75.2	120.1	241.8	190	-	427
Hydrogel C_1	78.5	151.5	263.5	188	-	415
Hydrogel C_2	71.9	111.7	289.5	241	-	421
Hydrogel C_3	88.5	146.1	280.8	183	-	425
Hydrogel D_1	103.4	161.5	275.2	181	250	418
Hydrogel D_2	91	143.3	302.3	266	-	433
Hydrogel D_3	71.9	118.2	273.6	180	255	429
Hydrogel E_1	75.7	131	245.7	195	-	352
Hydrogel E_2	104.5	157.7	301.1	279	-	432
Hydrogel E_3	81.7	142.5	268.6	199	269	443
Eudragit RSPO	273.9	343.4	382.7	-	-	387
Eudragit RL100	213.4	297.5	390.5	-	-	395
Eudragit S100	197.9	319.9	380.5	-	-	383
Eudragit L100	87.6	239.3	432.2	-	-	446
Eudragit L100-55	176.6	251.7	362.8	-	-	367
PVA	240.9	292	356.5	337	-	444
PVP	68.5	316.6	437.5	-	-	441
PEG	357.1	373.3	405.7	-	-	411
BSA	90.9	229.7	348.9	322	-	-
BSA-FITC	41.3	76.9	360.8	295	-	-

Figure S6 and **Table S3** contains the TGA plots and table summary. It has been observed that the temperature required for a 5% loss of weight changes dramatically from one formulation to another. In the case of empty hydrogels (scenario 1), hydrogels C and E lose 5% of their weight with temperatures in the range of 75 – 78 °C.

The materials hydrogels A, B, and D require temperatures above 100°C to lose weight, whereas hydrogels C and E show the same weight loss at lower temperatures. However, the differences between the materials decrease as more weight is lost. These findings align with the temperatures required for weight loss in Eudragit references, underscoring the critical role of this polymer in matrix formulations. Nevertheless, when BSA is

encapsulated in the hydrogels (scenario 2), the required temperature to eliminate 5% and 10% of weight decreases for hydrogels A - D, but increases for hydrogel E. This result suggests that BSA protein reinforces physical interactions between polymers in hydrogel E, making it more robust at higher temperatures. For 50% weight loss, the temperature required is higher in hydrogels B - E but lower in hydrogel A when BSA is present. This fact confirms that BSA protein can increase the stability of hydrogels, especially for more hydrophilic formulations (hydrogels C, D, and E). Hydrogel A is the most hydrophobic formulation, and instability could likely compromise the interactions between BSA and polymeric chains after losing half of its weight, decreasing the overall heating temperature.

In Scenario 3, BSA is chemically conjugated with a hydrophobic fluorophore (FITC), resulting in different tendencies compared to the previous case. Hence, the presence of a small hydrophobic molecule reinforces the physically cross-linked polymeric chain in hydrogels A, C, and E. As a result, the temperature required to remove half of the weight is higher than when the hydrogels are empty. Conversely, for hydrogels B and D, the temperature needed to lose half of the weight decreases slightly but remains similar to that of the empty hydrogels.

To better understand the results, we plotted the first derivative of the TGA curve and identified inflection points for differential thermal analysis. **Figure S6 F - J** shows the first derivative of the TGA curve for hydrogels A - E in the three scenarios previously discussed, along with the first derivative for the TGA curve of Eudragits, PVA, PEG, BSA, and BSA-FITC, which were used as references in our analysis. **Table S3** summarizes the maximum peaks obtained from the first derivative curve for each analysis, which have been divided into two regions for simplicity: Region 1 (100 – 350 °C) and Region 2 (350 – 700 °C).

In **Figure S6 F - J**, we can clearly see that Region 2 always contains a more prominent peak compared to Region 1. This result can be explained by looking at the calcination temperature for neat polymers in **Table S3**, where they all have it around 400°C. The peaks observed in Region 1 correspond to BSA and PVA. Furthermore, as seen in the figure, the maximum temperature values correlate with the hydrogels and BSA-FITC encapsulated in them.

Our findings showed that the presence of a hydrophobic molecule reinforced the intermolecular interactions within the hydrogels, and the encapsulation of proteins increased their stability.

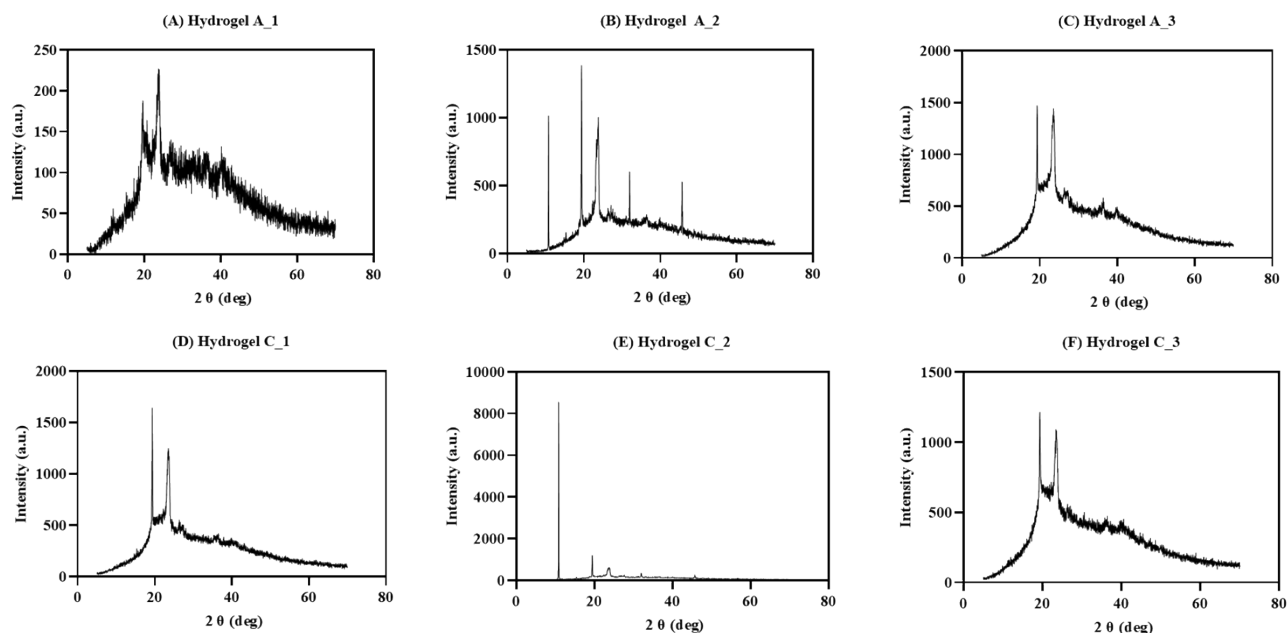## S4.3 Wide-angle X-ray scattering

Figure S7. WAXS analysis of (A) empty hydrogel A. (B) hydrogel A with BSA. (C) hydrogel A with BSA-FITC. (D) empty hydrogel C. (E) hydrogel C with BSA. (F) hydrogel C with BSA-FITC.

Table S4. Summary of PVA and PEG percentage of crystals presented in hydrogels A_1, A_3, C_1, and C_3.

Sample Code	Xc% (PVA)	Xc% (PEG)
Hydrogel A_1	1.58	2.06
Hydrogel A_3	1.69	4.09
Hydrogel C_1	1.61	3.42
Hydrogel C_3	1.52	2.35

Wide-angle X-ray scattering (WAXS) experiments were performed to check that the observed endotherms are mainly due to gel formation and not to crystals presence. WAXS measurements were performed on empty hydrogels A and C, as representative of the different Eudragit families, as well as hydrogels with BSA and BSA-FITC, respectively. **Figure S7** shows the data indicating that the hydrogels had an amorphous halo with several crystalline signals. Bragg peaks were observed at 19 and 23 degrees for all 6 formulations. Materials

with BSA (**Figure S7 B** and **E**) additionally had Bragg peaks at 10, 31, and 45 degrees. The reason for the presence of the extra signals is that BSA has been dissolved in the PBS buffer. During the gelation process, the inorganic salts were dried, thereby forming crystals. However, the intensity of signals at 19 and 23 degrees was lower for hydrogels A_2 and C_2 than for other formulations. For materials A_1, C_1, A_3, and C_3, no inorganic salts were used during the synthetic process to understand the salt effect properly. Hence, signals at 19 and 23 degrees belonged to polymeric crystals, specifically PVA crystals (19 degrees) and PEG crystals (23 degrees), as reported in previous studies.[7,8] The crystal fractions are summarized in **Table S4** by integrating the area under the curve for each peak and dividing it by the total area. We only determined the crystals fraction for scenarios 1 and 3, as scenario 2 could not be integrated properly. The data led us to conclude that all the formulations with more PEG are less crystalline than those with PVA.

However, the crystal fractions calculated by WAXS in **Table S4** are too small, which leads to the conclusion that the endothermic transitions observed by DSC mainly correspond to the gelation process with a very minor contribution from crystal melting, which should occur at similar temperatures.

It is worth mentioning that by adding BSA to the hydrogel, the enthalpy of the endothermic transition is reduced from 24.8 to 4.8 J/g. We have previously observed similar findings in the BSA kinetic release profiles (**Section 3.6**). The study demonstrated a significant interaction between the protein and Eudragits and PVP, causing these polymers to elute more rapidly from the hydrogel matrix. Consequently, this interaction reduces the formation of physical bonds between the polymers. Conversely, when BSA is chemically combined with FITC, the hydrogel becomes less soluble, increasing the enthalpy of the endothermic transition to 16.1 J/g. Similar results were seen in hydrogels B – E (**Section S4.1**), indicating that the presence of hydrophobic molecules during gelation increases the enthalpy of the gelation-related endotherms.

Supporting Information References

1   N. A. Peppas, *Makromol. Chemie*, 1975, **176**, 3433–3440.

2   J. L. Holloway, A. M. Lowman and G. R. Palmese, *Soft Matter*, 2013, **9**, 826–833.

3   J. Pushpamalar, P. Meganathan, H. L. Tan, N. A. Dahlan, L.-T. Ooi, B. N. H. M. Neerooa, R. Z. Essa, K. Shameli and S.-Y. Teow, *Gels*, 2021, **7**, 153.

4   A. S. Ahmed, U. K. Mandal, M. Taher, D. Susanti and J. M. Jaffri, *Pharm. Dev. Technol.*, 2018, **23**, 751–760.

5   S. Lefnaoui, N. Moulai-mostefa, M. M. Yahoum, S. N. Gasmi, S. Lefnaoui, N. Moulai-mostefa, M. M. Yahoum and S. N. Gasmi, *Drug Dev. Ind. Pharm.*, 2018, **44**, 432–443.

6   L. Greenspan, *J. Res. Natl. Bur. Stand. Sect. A Phys. Chem.*, 1977, **81A**, 89.

7   S. Lin, X. Liu, J. Liu, H. Yuk, H. Loh, G. A. Parada, C. Settens, J. Song, A. Masic, G. H. McKinley and X. Zhao, *Sci. Adv.*, 2019, **5**, 1–9.

8   M. K. Barron, T. J. Young, K. P. Johnston and R. O. Williams, *AAPS PharmSciTech*, 2003, **4**, 1–13.